Available online at www.sciencedirect.com
ScienceDirect
Journal 00 (2023) 1–21
Journal

Prestress estimation in elastic rods using dispersion-constrained inversion

Ngoc M. La[a], Cuong T. Nguyen[a,*], John L. Tassoulas[b]

[a]School of Science, Engineering and Technology, RMIT University Vietnam, Ho Chi Minh City, Vietnam
[b]Department of Civil, Architectural and Environmental Engineering,
The University of Texas at Austin, 1 University Station C1748, Austin, TX 78712, USA

Abstract

The theory of waveguides has been applied to various problems of engineering, including the evaluation of prestress in reinforced concrete members and non-destructive inspection or monitoring of long slender structures such as pipes and rails. In prestressed concrete beams or slabs, it is crucial to estimate the current level of prestress in the steel tendons for assessing the limit loads that these structural members can withstand. In this paper, we present a dispersion-constrained inversion for predicting the initial stress of circular-cross-section elastic rods on the basis of its harmonic torsional response. In the forward problem, the displacement is computed by implementing a hyper element representing the straight rod. The inversion problem is solved by optimizing the misfit function subjected to the dispersion constraints which are conveyed from the forward problem. The misfit function is defined as the L_2-norm of the difference between the measured and predicted responses and is minimized by means of gradient-based optimization. The gradient is derived in terms of derivatives with respect to the eigenvalues (wavenumbers), eigenvectors (mode shapes), Lagrange multipliers, and the prestress. We then estimate the prestress by solving the optimization problem through an iterative process. The proposed inversion is applied to several examples to examine its performance. Via these numerical examples, we demonstrate that our inverse algorithm can detect the prestress with satisfactory accuracy, even in the presence of noise in the measurements.

© 2023 Published by Elsevier Ltd.

Keywords: wave propagation, inverse problems, prestress, elastic rods

1. Introduction

Prestressed concrete is nowadays used extensively in civil structures such as bridges, tunnels, water tanks, roofs, piles, and other structures requiring long spans. By applying initial tension to the tendons, we aim to impart compression to concrete and, thereby, increase the structural integrity and avoid cracks in concrete. Nevertheless, the prestress level decreases over time due to steel relaxation, concrete deformation and other factors. These losses may entail serviceability issues and, in extreme cases, may even lead to structural collapse. Therefore, monitoring the level of pretension plays an important role in maintaining structural wellness. In manufacturing, residual stress has been noted as, possibly, affecting material performance. For biological tissue, the residual stress is used to self-adjust stresses and strains, thus leading to ideal mechanical conditions for the tissue. An important focus in these problems is the

*Corresponding author.
Email address: cuong.nguyentan@rmit.edu.vn (Cuong T. Nguyen)

effect of initial or residual stress on the subsequent behavior of elastic structures. In two articles [1] & [2] and one monograph [3], Biot presented the linear theory of elasticity of initially stressed solids and examined the influence of various types of prestress on elastic wave propagation. More recently, Destrade and Ogden [4] and Shams et al. [5] provided a general framework for studying the effects of initial stress on incremental deformation.

One approach towards prestress identification is to use dynamic response data recorded from vibration tests and, in the present study, we seek to minimize the misfit between measured and computed responses in the frequency domain. The prestress inversion problem belongs to the broader class of wave-driven inverse problems. These are usually cast in the context of a partial-differential-equation-constrained optimization framework, in which minimization of the objective functional, constrained by the underlying physics, leads to a prediction of the desired parameters. In principle, inverse problems are normally ill-posed due to the violation of Hadamard's conditions. Therefore, a regularized approach, e.g. Tikhonov regularization, is necessary to make the problem a well-posed one (Tadi [6], Na and Kallivokas [7], Karve et al. [8], Fathi et al. [9]). In Mashayekh et al.[10], estimating parameters in layered media is considered as an optimization problem constrained by the dispersion obtained from the associated forward problem. Similar problems were also addressed by Lee and Lee [11] who considered a layered half-space by applying mid-point integrated finite elements and perfectly matched discrete layers.

For the forward problem under consideration in this work, the displacement components are computed in the frequency domain using a semi-discrete finite element approach developed by Kocakaplan and Tassoulas [12] & [13]. The formulation was applied successfully to circular cross-section rods undergoing harmonic vibrations for both symmetric and antisymmetric modes. The wavemodes are discrete only in the radial direction but continuous axially and circumferentially. Using a Fourier series expansion of the displacement in the circumferential direction, the Kocakaplan and Tassoulas [12] obtained a quadratic eigenvalue problem and reduced the dimensionality of the problem to one from three, resulting in computational savings. In this work, we focus on detecting the level of initial stress in circular cross-section rods of finite length from its dynamic torsional response. In particular, we adapt the inverse framework presented in Mashayekh [10], to estimation of the rod pretension. The solution is obtained from the stationary point found by solving the Lagrangian problem incorporating the misfit between predicted and measured responses at a given angular frequency, imposing the dispersion relation (the quadratic eigenvalue problem) and the modal orthonormality condition.

There are two contributions in this work. First, we derive the closed-form expressions of matrices used in the quadratic eigenvalue problem for studying wave propagation in finite rods, then a semi-analytical solution for the displacement can be obtained. The second contribution is that we introduce a fairly simple algorithm helping us detect the initial stress from dynamic responses. In section 2, the governing equations for rods of circular cross-section in the forward problem are summarized while, in section 3, we present, in detail, the inversion algorithm to predict the pretension based on the dispersion constraint. Finally, the numerical results illustrating the performance of the proposed approach are discussed in section 4 and the conclusions are presented in section 5.

2. Forward problem

To prepare for the inversion method that uses dispersion as a constraint, the forward problem will be reviewed in this section. Most of the technical details to compute the displacement in the frequency domain can be found in two articles by Kocakaplan and Tassoulas ([12] & [13]). In our derivation, we provide the closed-form expressions of the matrices used in the quadratic eigenvalue problem (QEP). Furthermore, we simplify the final expression of the displacement aiming to further reduce the computational cost. This reduction is especially meaningful in the inverse problem.

2.1. Torsional wave modes

Considering antisymmetric modes (Fourier number $n = 0$) in a circular-cross-section rod of finite length, its torsional spectrum only involves the azimuthal (circumferential) displacement given by:

$$v(r, \theta, z) = V(r)\, e^{-ikz}. \tag{1}$$

Proceeding with the semidiscrete finite element method introduced by Kocakaplan and Tassoulas [12], we discretize the cross-section into N annuli. Specifically, there are $N + 1$ nodes as shown in Fig. 1 (right). We utilize linear interpolation in approximating the displacement field in each annulus over the interval $[R_i, R_{i+1}]$, $i = \overline{1, N}$ and $0 = R_1 < R_2 < ... < R_{N+1} = R$ being the rod radius. The harmonic factor $e^{i\omega t}$ is understood to multiply all field quantities. Implicitly, the mode shape $\boldsymbol{V}$ and the wavenumber k are functions of the frequency ω - in other words, these are time-harmonic modes at frequency ω.

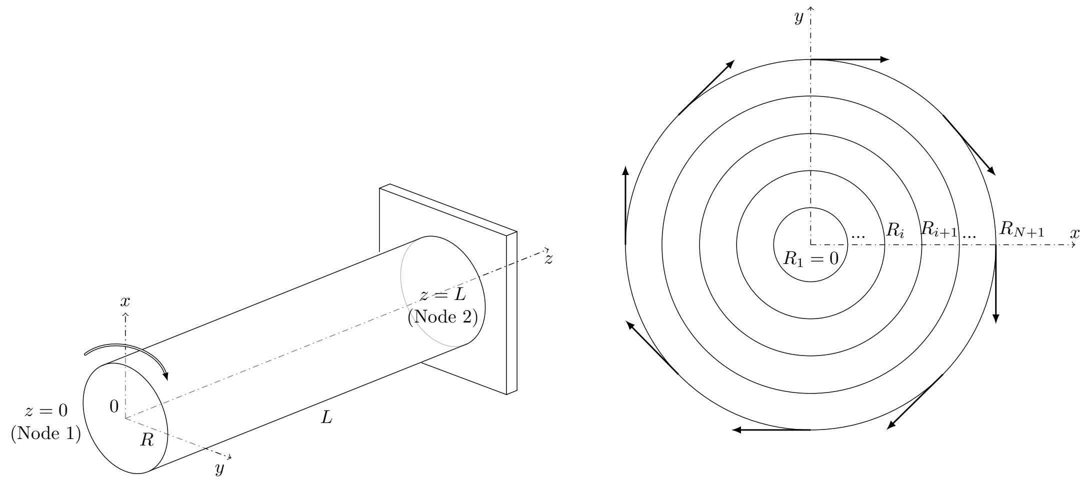

Figure 1: Rod of radius R and length L subjected to torque [13] (left) with its cross-section discretized into concentric annuli [12] (right).

Thus, we arrive at the following QEP with the wavenumber k (eigenvalue) and the mode shape $\boldsymbol{V}$ (the corresponding eigenvector).

$$\left[k^2\boldsymbol{A} + \boldsymbol{G} - \omega^2\boldsymbol{M}\right]\boldsymbol{V} = \boldsymbol{0}, \tag{2}$$

where

$$\boldsymbol{V} = \begin{bmatrix} V_1 & V_2 & \dots & V_{N+1} \end{bmatrix}^T, \tag{3}$$

and $\boldsymbol{A}$, $\boldsymbol{G}$ and $\boldsymbol{M}$ are tridiagonal $(N+1)$-by-$(N+1)$ matrices assembled from 2-by-2 annular counterparts $\boldsymbol{A}_i$, $\boldsymbol{G}_i$, $\boldsymbol{M}_i$, $i = 1, ..., N$ given below

$$\boldsymbol{A}_i = \gamma \int_{R_i}^{R_{i+1}} \boldsymbol{N}_i^T \boldsymbol{N}_i r dr, \qquad \gamma = \alpha_1 + (1+\beta_1) S_0, \tag{4}$$

$$\boldsymbol{G}_i = \alpha_1 \left(\int_{R_i}^{R_{i+1}} \frac{d\boldsymbol{N}_i^T}{dr}\frac{d\boldsymbol{N}_i}{dr} r dr - \int_{R_i}^{R_{i+1}} \frac{d\boldsymbol{N}_i^T}{dr}\boldsymbol{N}_i dr - \int_{R_i}^{R_{i+1}} \boldsymbol{N}_i^T \frac{d\boldsymbol{N}^i}{dr} dr + \int_{R_i}^{R_{i+1}} \boldsymbol{N}_i^T \boldsymbol{N}_i \frac{1}{r} dr \right), \tag{5}$$

$$\boldsymbol{M}_i = \rho \int_{R_i}^{R_{i+1}} \boldsymbol{N}_i^T \boldsymbol{N}_i r dr, \tag{6}$$

where

$$\boldsymbol{N}_i = \begin{bmatrix} \dfrac{R_{i+1} - r}{R_{i+1} - R_i} & \dfrac{r - R_i}{R_{i+1} - R_i} \end{bmatrix} \tag{7}$$

is the matrix of nodal interpolation functions in annulus i^{th} and $R_i < r < R_{i+1}$, while α_1 is the shear modulus, β_1 is a dimensionless coefficient (material property) and S_0 is the initial stress.

Denoting the thickness of annulus i by $\Delta R_i = R_{i+1} - R_i$, Eqs. (7) can be rewritten as:

$$\boldsymbol{N}_i = \frac{1}{\Delta R_i}\begin{bmatrix} R_{i+1} - r & r - R_i \end{bmatrix}. \tag{8}$$

Therefore, its derivative is given by:

$$\frac{d\boldsymbol{N}_i}{dr} = \frac{1}{\Delta R_i}\begin{bmatrix} -1 & 1 \end{bmatrix}. \tag{9}$$

At any given frequency, the eigenvalue problem in Eq. (2) admits $2(N+1)$ eigenvalues (the wavenumbers k) corresponding $2(N+1)$ eigenvectors (modes $\boldsymbol{V}$). The $2(N+1)$ eigenvalues are arranged in $N+1$ pairs of the form $(k, -k)$. Since $\boldsymbol{A}$ and $\boldsymbol{M}$ are positive definite while $\boldsymbol{G}$ is positive semi-definite, the wavenumbers are either imaginary or real. We collect all modes that propagate or decay in the positive $z-$ direction. In particular, from each pair $(k, -k)$, the wavenumber with positive real part or negative imaginary part will be retained and arranged into a diagonal matrix of wavenumbers:

$$\boldsymbol{K} = diag\left[k_j, j = \overline{1, N+1}\right]. \tag{10}$$

For computational purposes, it is convenient to derive the closed-form expressions of the integrals arising in the expressions of matrices $\boldsymbol{A}_i, \boldsymbol{G}_i$ and $\boldsymbol{M}_i$. Specifically, with regard to $\boldsymbol{A}_i$, we have:

$$\boldsymbol{N}_i^T\boldsymbol{N}_i = \frac{1}{(\Delta R_i)^2}\begin{bmatrix} (R_{i+1} - r)^2 & (R_{i+1} - r)(r - R_i) \\ sym & (r - R_i)^2 \end{bmatrix} = \begin{bmatrix} I_1 & I_2 \\ I_2 & I_3 \end{bmatrix}, \tag{11}$$

where:

$$I_1 = \frac{(R_{i+1} - r)^2}{(\Delta R_i)^2}, \quad I_2 = \frac{(R_{i+1} - r)(r - R_i)}{(\Delta R_i)^2}, \quad I_3 = \frac{(r - R_i)^2}{(\Delta R_i)^2}. \tag{12}$$

Then, the matrix $\boldsymbol{A}_i$ can be written in terms of the above three integrals as:

$$\boldsymbol{A}_i = \gamma \int_{R_i}^{R_{i+1}} \begin{bmatrix} I_1 & I_2 \\ I_2 & I_3 \end{bmatrix} rdr. \tag{13}$$

The three integrals I_1, I_2, I_3 can be evaluated explicitly as follows:

$$\int_{R_i}^{R_{i+1}} I_1 rdr = \frac{R_{i+1}^2}{12} + \frac{R_{i+1}R_i}{6} - \frac{R_i^2}{4}, \int_{R_i}^{R_{i+1}} I_2 rdr = \frac{1}{12}\left(R_{i+1}^2 - R_i^2\right), \int_{R_i}^{R_{i+1}} I_3 rdr = \frac{R_{i+1}^2}{4} - \frac{R_{i+1}R_i}{6} - \frac{R_i^2}{12}. \tag{14}$$

Similarly, the matrix $\boldsymbol{M}_i$ can be written in terms of I_1, I_2, I_3 as follows

$$\boldsymbol{M}_i = \rho \int_{R_i}^{R_{i+1}} \begin{bmatrix} I_1 & I_2 \\ I_2 & I_3 \end{bmatrix} rdr. \tag{15}$$

We write $\boldsymbol{G}_i$ in terms of four matrices denoted by $\boldsymbol{G}_{i1}, \boldsymbol{G}_{i2}, \boldsymbol{G}_{i3}$, and $\boldsymbol{G}_{i4}$, in the order appearing in Eq. (5):

$$\boldsymbol{G}_{i1} = \alpha_1 \int_{R_i}^{R_{i+1}} \frac{d\boldsymbol{N}_i^T}{dr}\frac{d\boldsymbol{N}_i}{dr} r dr = \alpha_1 \int_{R_i}^{R_{i+1}} \frac{1}{(\Delta R_i)^2}\begin{bmatrix} 1 & -1 \\ -1 & 1 \end{bmatrix} r dr = \alpha_1 \int_{R_i}^{R_{i+1}} \begin{bmatrix} I_4 & -I_4 \\ -I_4 & I_4 \end{bmatrix} r dr, \tag{16}$$

$$\boldsymbol{G}_{i2} = -\alpha_1 \int_{R_i}^{R_{i+1}} \frac{d\boldsymbol{N}_i^T}{dr}\boldsymbol{N}_i dr = \alpha_1 \int_{R_i}^{R_{i+1}} \frac{1}{(\Delta R_i)^2}\begin{bmatrix} R_{i+1}-r & -(R_i - r) \\ -(R_{i+1}-r) & R_i - r \end{bmatrix} dr = \alpha_1 \int_{R_i}^{R_{i+1}} \begin{bmatrix} I_5 & -I_6 \\ -I_5 & I_6 \end{bmatrix} dr, \tag{17}$$

$$\boldsymbol{G}_{i3} = -\alpha_1 \int_{R_i}^{R_{i+1}} \boldsymbol{N}_i^T \frac{d\boldsymbol{N}^i}{dr} dr = \boldsymbol{G}_2^T, \tag{18}$$

$$\boldsymbol{G}_{i4} = \alpha_1 \int_{R_i}^{R_{i+1}} \boldsymbol{N}_i^T \boldsymbol{N}_i \frac{1}{r} dr = \int_{R_i}^{R_{i+1}} \begin{bmatrix} I_1 & I_2 \\ I_2 & I_3 \end{bmatrix} \frac{1}{r} dr, \tag{19}$$

where:

$$I_4 = \frac{1}{(\Delta R_i)^2}, \qquad I_5 = \frac{R_{i+1}-r}{(\Delta R_i)^2}, \qquad I_6 = \frac{R_i - r}{(\Delta R_i)^2}. \tag{20}$$

Then, the above integration can be computed as:

$$\int_{R_i}^{R_{i+1}} I_4 r dr = \frac{R_{i+1}+R_i}{2(\Delta R_i)}, \quad \int_{R_i}^{R_{i+1}} I_5 dr = \frac{1}{2}, \quad \int_{R_i}^{R_{i+1}} I_6 dr = \frac{-1}{2}, \tag{21}$$

$$\int_{R_i}^{R_{i+1}} I_1 \frac{1}{r} dr = \frac{R_i^2 - 2R_{i+1}^2 \log \dfrac{R_{i+1}}{R_i} - 4R_i R_{i+1} + 3R_{i+1}^2}{2(\Delta R_i)^2}, \tag{22}$$

$$\int_{R_i}^{R_{i+1}} I_2 \frac{1}{r} dr = \frac{-R_i^2 - 2R_i R_{i+1} log \dfrac{R_{i+1}}{R_i} + R_{i+1}^2}{2(\Delta R_i)^2}, \tag{23}$$

$$\int_{R_i}^{R_{i+1}} I_3 \frac{1}{r} dr = \frac{3R_i^2 + 2R_i^2 \log \dfrac{R_{i+1}}{R_i} - 4R_{i+1} R_i + R_{i+1}^2}{2(\Delta R_i)^2}. \tag{24}$$

Remark. For the purpose of implementation, if an uniform mesh is used, the annular thickness $\Delta R_i = R_{i+1} - R_i$, $i = 1, ..., N$ will be constant, leading to a simplification in the above expressions. Furthermore, it is worth noting that we use the midpoint rule for Eqs. (22), (23), and (24) for estimating $\boldsymbol{G}_{i4}$ at the first annulus to get rid of the singularity occuring when $R_1 = 0$. In particular, at this annulus ($(i = 1)$) we focus on the value of $\boldsymbol{G}_{i4}$:

$$\boldsymbol{G}_{14} = \alpha_1 \int_{R_1}^{R_2} \begin{bmatrix} I_1 & I_2 \\ I_2 & I_3 \end{bmatrix} \frac{1}{r} dr = \int_{R_1}^{R_2} I_7(r)\, dr. \tag{25}$$

The first thickness ΔR_1 is divided into n subintervals to approximate $\boldsymbol{G}_{14}$. Let $dR = \dfrac{\Delta R_1}{n}$, the midpoints of the n subintervals are:

$$\left\{R_1 + \frac{1}{2}dR, R_1 + \frac{3}{2}dR, R_1 + \frac{5}{2}dR, ...\right\} = R_1 + \left(m - \frac{1}{2}\right)dR, \quad m = \overline{1, n}.$$

Thus,

$$\boldsymbol{G}_{14} \simeq \sum_{m=1}^{n} I_7 \left(R_1 + \left(m - \frac{1}{2} \right) dR \right) dR. \tag{26}$$

2.2. *Hyper element*

We consider a finite rod of length L subjected to torque at one end and fixed at the other. Following the procedure presented in Kocakaplan and Tassoulas [13], the rod segment is analyzed as a hyper element with two nodes: node 1 at $z = 0$ and node 2 at $z = L$ shown in Fig. 1 (left).

Now, we obtain the dynamic stiffness matrix for this hyper element. Considering all modes which are traveling or decaying in the positive or the negative z-direction, the displacement vectors at nodes 1 ($z = 0$) and 2 ($z = L$) can be combined into the following displacement vector for the entire hyper element:

$$\boldsymbol{\mathcal{V}} = \begin{bmatrix} \boldsymbol{\mathcal{V}}_1 \\ \boldsymbol{\mathcal{V}}_2 \end{bmatrix} = \boldsymbol{X} \begin{bmatrix} \boldsymbol{I} & \boldsymbol{E} \\ \boldsymbol{E} & \boldsymbol{I} \end{bmatrix} \boldsymbol{\Gamma}, \qquad \text{where } \boldsymbol{\Gamma} = \begin{bmatrix} \boldsymbol{\Gamma}_+ \\ \boldsymbol{\Gamma}_- \end{bmatrix}, \tag{27}$$

in which $\boldsymbol{\Gamma}_+, \boldsymbol{\Gamma}_-$ are the vectors of participation vectors of the modes in the positive and negative z-directions, respectively. Meanwhile, $\boldsymbol{X}$ is the matrix of $N + 1$ eigenvectors $\boldsymbol{X}_i$:

$$\boldsymbol{X} = \left[\boldsymbol{V}^{(1)}, \boldsymbol{V}^{(2)}, ..., \boldsymbol{V}^{(N+1)} \right]. \tag{28}$$

$\boldsymbol{\mathcal{V}}_1$ and $\boldsymbol{\mathcal{V}}_2$ are the vectors of circumferential displacements at nodes 1 and 2:

$$\boldsymbol{\mathcal{V}}_1 = \begin{bmatrix} v\,(z = 0, r = R_1) \\ v\,(z = 0, r = R_2) \\ \vdots \\ v\,(z = 0, r = R_{N+1}) \end{bmatrix}, \boldsymbol{\mathcal{V}}_2 = \begin{bmatrix} v\,(z = L, r = R_1) \\ v\,(z = L, r = R_2) \\ \vdots \\ v\,(z = L, r = R_{N+1}) \end{bmatrix}. \tag{29}$$

$$\boldsymbol{E} = \operatorname{diag}\left[\exp\left(-ik_j L \right), j = \overline{1, N+1} \right]. \tag{30}$$

If torque is applied at the near end, it is clear that there will be only shear stress $\tau_{z\theta}$ for a mode $(\omega, k, \boldsymbol{V})$ on any cross-section of the rod, it can be computed as

$$\tau_{z\theta} = \gamma \frac{\partial v}{\partial z} = -\mathrm{i}k\gamma \boldsymbol{N}\boldsymbol{V} \exp\left(-\mathrm{i}kz \right), \tag{31}$$

where $\boldsymbol{N}$ is the global matrix of local interpolation functions in each annulus.

The nodal force can be expressed as:

$$\boldsymbol{P} = \begin{bmatrix} \boldsymbol{P}_1 \\ \boldsymbol{P}_2 \end{bmatrix} = \mathrm{i}k\gamma \begin{bmatrix} 1 \\ -\exp\left(-ikL \right) \end{bmatrix} \int_0^R \boldsymbol{N}^T \boldsymbol{N}\boldsymbol{V} dr d\theta. \tag{32}$$

From Eq. (4), the nodal forces can be rewritten as

$$\boldsymbol{P} = 2\pi \mathrm{i}k \begin{bmatrix} 1 \\ -\exp\left(-ikL \right) \end{bmatrix} \boldsymbol{A}\boldsymbol{V}. \tag{33}$$

Combining modes traveling or decaying in the positive and negative z directions, the nodal forces can be expressed in terms of these modes as follows:

$$\boldsymbol{P} = 2\pi \mathrm{i} \boldsymbol{A}\boldsymbol{X}\boldsymbol{K} \begin{bmatrix} \boldsymbol{\Gamma}^+ - \boldsymbol{E}\boldsymbol{\Gamma}^- \\ -\boldsymbol{E}\boldsymbol{\Gamma}^+ + \boldsymbol{\Gamma}^- \end{bmatrix} = 2\pi \mathrm{i} \boldsymbol{A}\boldsymbol{X}\boldsymbol{K} \begin{bmatrix} \boldsymbol{I} & -\boldsymbol{E} \\ -\boldsymbol{E} & \boldsymbol{I} \end{bmatrix} \boldsymbol{\Gamma} \tag{34}$$

The nodal force and nodal displacement of the hyper element are related via the dynamic stiffness matrix $\boldsymbol{H}$:

$$\boldsymbol{P} = \boldsymbol{H}\boldsymbol{V}, \tag{35}$$

where:

$$\boldsymbol{H} = 2\pi \mathrm{i}\boldsymbol{A}\boldsymbol{X}\boldsymbol{K}\begin{bmatrix}\boldsymbol{I} & -\boldsymbol{E}\\ -\boldsymbol{E} & \boldsymbol{I}\end{bmatrix}\begin{bmatrix}\boldsymbol{I} & \boldsymbol{E}\\ \boldsymbol{E} & \boldsymbol{I}\end{bmatrix}^{-1}\boldsymbol{X}^{-1}. \tag{36}$$

2.3. Torsional stiffness

In this study, a Neumann boundary condition is applied as shown in Fig. 1 (left), in which only the edge of the initial cross-section ($z = 0, r = R$) is subjected to uniformly distributed azimuthal traction, while the traction vanishes on the rest of the cross-section. Therefore, the force at node 1 can be set equal to:

$$\boldsymbol{P}_1 = \begin{cases} 1 & \text{at the edge} \\ 0 & \text{otherwise.}\end{cases} \tag{37}$$

We now use the stiffness matrix $\boldsymbol{H}$ to compute the azimuthal displacement only at node 1. From Eq. (36), matrix $\boldsymbol{H}$ can be simplified further as:

$$\boldsymbol{H} = 2\pi \mathrm{i}\boldsymbol{A}\boldsymbol{X}\boldsymbol{K}\begin{bmatrix}\boldsymbol{I}+\boldsymbol{E}^2 & -2\boldsymbol{E}\\ -2\boldsymbol{E} & \boldsymbol{I}+\boldsymbol{E}^2\end{bmatrix}\left(\boldsymbol{I}-\boldsymbol{E}^2\right)^{-1}\boldsymbol{X}^{-1}. \tag{38}$$

For the sake of simplicity, the matrix $\boldsymbol{H}$ can be considered as a 2×2 block-matrix. To determine the displacement vector at node 1, we only need the first element of $\boldsymbol{H}$:

$$\boldsymbol{H}_{11} = 2\pi i\boldsymbol{A}\boldsymbol{X}\boldsymbol{K}\boldsymbol{D}\boldsymbol{X}^{-1}, \tag{39}$$

where:

$$\boldsymbol{D} = \left(\boldsymbol{I}+\boldsymbol{E}^2\right)\left(\boldsymbol{I}-\boldsymbol{E}^2\right)^{-1}. \tag{40}$$

Then, the inverse of $\boldsymbol{H}_{11}$ can be computed easily as

$$\boldsymbol{H}_{11}^{-1} = \frac{1}{2\pi i}\boldsymbol{X}\boldsymbol{Z}\boldsymbol{X}^{-1}\boldsymbol{A}^{-1}, \tag{41}$$

where $\boldsymbol{Z} = \boldsymbol{D}^{-1}\boldsymbol{K}^{-1}$.

In order to obtain a semi-analytical solution for the displacement, we start by simplifying matrix $\boldsymbol{D}$. Specifically, $\boldsymbol{I} \pm \boldsymbol{E}^2$ can be rewritten in terms of the following diagonal matrices:

$$\boldsymbol{I}+\boldsymbol{E}^2 = \mathrm{diag}\left[1+\exp\left(-2ik_jL\right)\right], \qquad \boldsymbol{I}-\boldsymbol{E}^2 = \mathrm{diag}\left[1-\exp\left(-2ik_jL\right)\right]. \tag{42}$$

Therefore, $\boldsymbol{D}$ is also a diagonal matrix:

$$\boldsymbol{D} = \mathrm{diag}\left[\frac{1+\exp\left(-2ik_jL\right)}{1-\exp\left(-2ik_jL\right)}\right]. \tag{43}$$

By applying Euler's formula, i.e., $\exp(i\theta) = \cos(\theta) + i\sin(\theta)$, $\boldsymbol{Z}$ can be expressed as:

$$\boldsymbol{Z} = \mathrm{diag}\left[\frac{1}{k_j}\frac{1-\exp\left(-2ik_jL\right)}{1+\exp\left(-2ik_jL\right)}\right] = \mathrm{diag}\left[\frac{i\tan\left(k_jL\right)}{k_j}\right]. \tag{44}$$

Finally, the displacement vector at node 1 can be computed as

$$\boldsymbol{V}_1 = \boldsymbol{H}_{11}^{-1}\boldsymbol{P}_1 = \frac{1}{2\pi i}\boldsymbol{X}\boldsymbol{Z}\boldsymbol{X}^{-1}\boldsymbol{A}^{-1}\boldsymbol{P}_1. \tag{45}$$

Since we wish to compute the outermost circumferential displacement, $v\,(r = R_{N+1}, z = 0) = \mathcal{V}_{1,N+1}$, only the last row of the $\boldsymbol{XZX}^{-1}$ term and the last column of $\boldsymbol{A}^{-1}$ need to be considered.

First, let us examine the following matrices:

$$\boldsymbol{X} = \left[\boldsymbol{V}^{(1)}, \boldsymbol{V}^{(2)}, \cdots, \boldsymbol{V}^{(N+1)}\right] = \begin{bmatrix} \vdots & \vdots & \cdots & \vdots \\ \vdots & \vdots & \cdots & \vdots \\ V_1 & V_2 & \cdots & V_{N+1} \end{bmatrix}, \tag{46}$$

$$\boldsymbol{Z} = \begin{bmatrix} Z_1 & \vdots & \vdots \\ \vdots & \ddots & \vdots \\ \vdots & \vdots & Z_{N+1} \end{bmatrix}, \tag{47}$$

and

$$\boldsymbol{X}^{-1} = \left[\boldsymbol{V}'_1, \boldsymbol{V}'_2, \cdots, \boldsymbol{V}'_{N+1}\right], \tag{48}$$

in which $\boldsymbol{V}'_i$ is the i-column of the inversion of matrix $\boldsymbol{X}$ for $i = \overline{1, N+1}$.

The matrix products can be written as:

$$\begin{aligned} \boldsymbol{XZX}^{-1} &= \begin{bmatrix} \vdots & \vdots & \cdots & \vdots \\ \vdots & \vdots & \cdots & \vdots \\ V_1 & V_2 & \cdots & V_{N+1} \end{bmatrix} \begin{bmatrix} Z_1 & \vdots & \vdots \\ \vdots & \ddots & \vdots \\ \vdots & \vdots & Z_{N+1} \end{bmatrix} \begin{bmatrix} \boldsymbol{V}'_1 & \boldsymbol{V}'_2 & \cdots & \boldsymbol{V}'_{N+1} \end{bmatrix} \\ &= \begin{bmatrix} \vdots & \vdots & \cdots & \vdots \\ \vdots & \vdots & \cdots & \vdots \\ V_1 Z_1 & V_2 Z_2 & \cdots & V_{N+1} Z_{N+1} \end{bmatrix} \begin{bmatrix} \boldsymbol{V}'_1 & \boldsymbol{V}'_2 & \cdots & \boldsymbol{V}'_{N+1} \end{bmatrix} \\ &= \begin{bmatrix} \vdots & \vdots & \cdots & \vdots \\ \vdots & \vdots & \cdots & \vdots \\ \sum V_i Z_i V'_{i1} & \sum V_i Z_i V'_{i2} & \cdots & \sum V_i Z_i V'_{i,N+1} \end{bmatrix}. \end{aligned} \tag{49}$$

Then, the last term in the expression of the circumferential displacement at $z = 0$, $\mathcal{V}_{1,N+1}$ can be computed as:

$$\begin{aligned} v\,(r = R_{N+1}, z = 0) = &\frac{1}{2\pi \mathrm{i}} \left[\left(\sum_{i=1}^{N+1} V_i Z_i V'_{i1}\right) a'_{1,N+1} + \left(\sum_{i=1}^{N+1} V_i Z_i V'_{i2}\right) a'_{2,N+1} + \cdots \right. \\ &\left. + \left(\sum_{i=1}^{N+1} V_i Z_i V'_{i,N+1}\right) a'_{N+1,N+1}\right], \end{aligned} \tag{50}$$

where the last column of $\boldsymbol{A}^{-1}$ is defined by $\begin{bmatrix} a'_{1,N+1} \\ a'_{2,N+1} \\ \vdots \\ a'_{N+1,N+1} \end{bmatrix}$.

3. Inverse problem

In this study, the objective is to use the outermost azimuthal displacement for predicting the level of prestress in the circular cross-section rod considered in the preceding section. It is assumed that the mass density ρ, the shear modulus α_1 (is also denoted by G) and the material coefficient β_1 are known. In practice, over a certain range of the angular frequency ω, the circumference displacement at the near end $v(z = 0, r = R;\, \omega)$ can be measured. As usual, the starting point in nearly all inverse problems is the construction of a misfit function computed as the square of the difference between the measured and predicted responses. The predicted prestress is determined via an iterative process that reduces the misfit value below a prescribed tolerance. The misfit function F is defined as:

$$F := \frac{1}{2}\left|v_m\,(0, R;\, \omega) - v_p\,(0, R;\, \omega)\right|^2, \tag{51}$$

where $v_p\,(0, R;\, \omega)$ denotes the predicted displacement with respect to the angular frequency ω and evaluated at position R and $v_m\,(0, R;\, \omega)$ denotes the measured displacement at the same point and the same frequency. Notice that we only consider the last term of the circumferential displacement vector at $z = 0$, which is calculated by Eq. (50).

During the prestress inversion iterations, to respect the physics of the problem under consideration, the misfit function is modified by adding physical laws as additional constraints. In general, the physical conditions can be imposed in many ways. Herein, the discrete quadratic eigenvalue problem described by Eq. (2), accompanied by the orthonormality condition is our choice for incorporating physical laws to the misfit function. We then arrive at a constrained optimization problem in which the Lagrange multiplier method can be utilized to include the dispersion into our minimization. In particular, we wish to find the minimum of misfit function F subjected to the dispersion constraint C:

$$L := F + C = \frac{1}{2}\left|v_m\,(0, R;\, \omega) - v_p\,(0, R;\, \omega)\right|^2 + C, \tag{52}$$

where C is defined as:

$$C = \mathrm{Re}\left\{\boldsymbol{\lambda}\left(k^2\boldsymbol{A} + \boldsymbol{G} - \omega^2\boldsymbol{M}\right)\boldsymbol{V} + \varphi\left(k\boldsymbol{V}^T\boldsymbol{A}\boldsymbol{V} - k\right)\right\}, \tag{53}$$

$\boldsymbol{\lambda}$ is a vector of Lagrange multipliers employed to incorporate the quadratic eigenvalue problem, and φ is a scalar Lagrange multiplier used for the modification by adding the orthonormality condition. In this study, the level of prestress S_0 is determined by minimizing the proposed misfit function (52).

Eq. (52) can be written in Lagrangian form:

$$L \equiv L\left(\boldsymbol{\lambda}, \varphi, \boldsymbol{V}, k, S_0\right), \tag{54}$$

where the Lagrangian functional is in terms of the Lagrange multipliers $\boldsymbol{\lambda}$ and φ, the state variables $\boldsymbol{V}$ and k, and the initial stress S_0.

Minimizing the functional introduced in Eq. (52) is equivalent to finding a stationary point for L. To do so, we set the first variation of L to zero:

$$\delta L\left(\boldsymbol{\lambda}, \varphi, \boldsymbol{V}, k, S_0\right) = \delta F + \delta C = 0, \tag{55}$$

or

$$\nabla L = \begin{bmatrix} \delta_{\boldsymbol{\lambda},\varphi} L \\ \delta_{\boldsymbol{V},k} L \\ \delta_{S_0} L \end{bmatrix} = 0. \tag{56}$$

3.1. State Problem

Taking the variations of the Lagrangian functional L with respect to the Lagrange multipliers (adjoint variables) $\boldsymbol{\lambda}$ and φ and requiring them to be zero, we obtain:

$$\delta_\lambda L = 0 \Rightarrow \left(k^2 \boldsymbol{A} + \boldsymbol{G} - \omega^2 \boldsymbol{M}\right) \boldsymbol{V} = 0. \quad (57)$$

Eq. (57) recovers the forward eigenvalue problem in Eq. (2)

$$\delta_\varphi L = 0 \Rightarrow k\boldsymbol{V}^T \boldsymbol{A}\boldsymbol{V} - k = 0 \quad \text{or} \quad \boldsymbol{V}^T \boldsymbol{A}\boldsymbol{V} = 1. \quad (58)$$

3.2. Adjoint problem

The solution of the state problem has been presented and the j^{th}-mode eigenvector $\boldsymbol{V}_j$ and eigenvalue k_j can be identified from Eqs. (57) and (58) and will then be employed to solve the "adjoint problem" of the Lagrange function. Similarly, the vanishing of the variations of L with respect to the state variables (the wavenumbers k and the eigenvectors $\boldsymbol{V}$) is applied, which results in:

$$\delta_{\boldsymbol{V}} L = 0 \Rightarrow \operatorname{Re}\left\{\frac{1}{2\pi}\sum_{i=1}^{N+1}\sum_{j=1}^{N+1} H_{1j} V'_{ji} a'_{i,N+1} \left(\overline{v_p - v_m}\right) \boldsymbol{W}^T \delta\boldsymbol{V}\right\} + \operatorname{Re}\left\{\boldsymbol{\lambda}^T \left(k^2 \boldsymbol{A} + \boldsymbol{G} - \omega^2 \boldsymbol{M}\right)\delta\boldsymbol{V} + 2k\varphi \boldsymbol{V}^T \boldsymbol{A}^T \delta\boldsymbol{V}\right\} = 0, \quad (59)$$

or

$$\left(k^2 \boldsymbol{A} + \boldsymbol{G} - \omega^2 \boldsymbol{M}\right)^T \boldsymbol{\lambda} + 2k\boldsymbol{A}\boldsymbol{V}\varphi = -\frac{1}{2\pi}\sum_{i=1}^{N+1}\sum_{j=1}^{N+1} H_{1j} V'_{ji} a'_{i,N+1} \left(\overline{v_p - v_m}\right) \boldsymbol{W}, \quad (60)$$

where $\boldsymbol{W}$ has unit only for displacement at $r = R_{N+1}$, whereas the other elements are nil, and

$$\delta_k L = 0 \Rightarrow \operatorname{Re}\left\{\frac{1}{2\pi}\sum_{i=1}^{N+1}\sum_{j=1}^{N+1} V_j H_{2j} V'_{ji} a'_{i,N+1} \left(\overline{v_p - v_m}\right)\delta k\right\} + \operatorname{Re}\left\{2k\boldsymbol{\lambda}^T \boldsymbol{A}\boldsymbol{V}\delta k + \varphi\left(\boldsymbol{V}^T \boldsymbol{A}\boldsymbol{V} - 1\right)\delta k\right\} = 0, \quad (61)$$

or

$$2k\boldsymbol{V}^T \boldsymbol{A}^T \boldsymbol{\lambda} + \left(\boldsymbol{V}^T \boldsymbol{A}\boldsymbol{V} - 1\right)\varphi = -\frac{1}{2\pi}\sum_{i=1}^{N+1}\sum_{j=1}^{N+1} V_j H_{2j} V'_{ji} a'_{i,N+1} \left(\overline{v_p - v_m}\right). \quad (62)$$

Combining Eq. (60) and Eq. (62), we obtain a symmetric system of $N+1$ linear equations:

$$\begin{bmatrix} \left(k_j^2 \boldsymbol{A} + \boldsymbol{G} - \omega^2 \boldsymbol{M}\right)^T & 2k_j \boldsymbol{A}\boldsymbol{V}_j \\ 2k_j \boldsymbol{V}_j^T \boldsymbol{A}^T & \boldsymbol{V}_j^T \boldsymbol{A}\boldsymbol{V}_j - 1 \end{bmatrix} \begin{bmatrix} \boldsymbol{\lambda}_j \\ \varphi_j \end{bmatrix} = -\frac{1}{2\pi}\begin{bmatrix} \sum_{i=1}^{N+1}\sum_{j=1}^{N+1} H_{1j} V'_{ji} a'_{i,N+1}\left(\overline{v_p - v_m}\right)\boldsymbol{W} \\ \sum_{i=1}^{N+1}\sum_{j=1}^{N+1} V_j H_{2j} V'_{ji} a'_{i,N+1}\left(\overline{v_p - v_m}\right) \end{bmatrix}, j = \overline{1, N+1}, \quad (63)$$

where k_j and $\boldsymbol{V}_j$ are the eigenvalue and eigenvector for the j^{th} mode, respectively.

3.3. Control problem

A gradient-based optimization technique is employed for the minimization of the Lagrange function L. The desired variation of L with respect to initial stress S_0 is given as follows:

$$\delta_{S_0} L = \operatorname{Re}\left\{\sum_{j=1}^{N+1} k_j^2 \boldsymbol{\lambda}_j^T \frac{\partial \boldsymbol{A}}{\partial S_0}\boldsymbol{V}_j + k_j \varphi_j \boldsymbol{V}_j^T \frac{\partial \boldsymbol{A}}{\partial S_0}\boldsymbol{V}_j\right\}\delta S_0. \quad (64)$$

It is worth noting that only matrix $\boldsymbol{A}$ depends upon S_0 as can be seen in Eq. (4).

The reduced gradient of the Lagrangian in Eq. (64) is given by:

$$\nabla_{S_0} L = \mathrm{Re}\left\{\sum_{j=1}^{N+1} k_j^2 \boldsymbol{\lambda}_j^T \frac{\partial \boldsymbol{A}}{\partial S_0} \boldsymbol{V}_j + k_j \varphi_j \boldsymbol{V}_j^T \frac{\partial \boldsymbol{A}}{\partial S_0} \boldsymbol{V}_j\right\} \tag{65}$$

and will be used to update the initial stress S_0 during the inversion iterations. The detailed derivation is given in Appendix A and Appendix B.

3.4. Inversion process

To reveal the initial stress S_0 through the iterative process, we begin with an assumed initial guess of S_0, and specify the excitation frequency ω. First, we solve the state problem in Eqs. (57) and (58) to determine $(N + 1)$ wavenumbers k corresponding to $(N + 1)$ eigenvectors $\boldsymbol{V}$. Consistently with Eq. (50), we use k and $\boldsymbol{V}$ to calculate the predicted displacement v_p, as well as the misfit value $\left|v_p - v_m\right|$. Then, solving the adjoint problem, for each j^{th} mode eigenvalue k_j and eigenvector $\boldsymbol{V}_j$, we arrive at the adjoint variables $\boldsymbol{\lambda}_j$ and φ_j. Next, using the adjoint and state variables, we compute the reduced gradient in Eq. (65). To update the initial guess S_0, we denote by $S_0^{(n)}$ and grad $S_0^{(n)}$ the values of the predicted S_0 and reduced gradient $\nabla_{S_0} L$ at the n^{th} inversion iteration, respectively:

$$S_0^{(n+1)} = S_0^{(n)} + \Delta S_0 \,\mathrm{grad}\, S_0^{(n)}, \tag{66}$$

where ΔS_0 is the step length.

Remark: For the $N + 1$ modes from the QEP,

$$\left[k_j^2 \boldsymbol{A} + \boldsymbol{G} - \omega^2 \boldsymbol{M}\right] \boldsymbol{V}_j = \boldsymbol{0}, \quad j = \overline{1, N+1}.$$

a normalization of the eigenvectors was chosen, similar to the one used by Waas [14], Kausel [15], and Mashayekh et al. [10],

$$\boldsymbol{V}_j^T \boldsymbol{A} \boldsymbol{V}_j = 1, \quad j = \overline{1, N+1}. \tag{67}$$

It should be noted that the eigenvalue problem in Eq. (2) and the orthonormality condition in Eq. (67) stand for the physics of the problem and constitute the forward or state problem, respectively. These equations are enforced as the misfit is minimized.

4. Numerical results

In our numerical experiments, the geometric and material parameters are set as follows: the rod segment is of radius R and its length $L = 100R$, which is a sufficiently long segment for practical applications; the mass density $\rho = 1$, the shear modulus $\alpha_1 = 1$, and β_1 can be either 0 or -0.5. In the finite-element computation, the rod cross-section is discretized using $N = 50$ annuli of equal radial dimension $\Delta R_i = R/50$. Other numerical parameters in our inverse process are chosen as in Table 1 with the maximum number of iterations *maxiter* = 2000. To demonstrate the performance of the dispersion-constrained inversion discussed in the preceding section, we first carry out numerical tests with the excitation frequency $\omega = 0.2$ in the ideal scenario, in which we assume that the measurement is noise-free. Then, we test our proposed algorithm with a set of four different frequencies $\omega = \{0.5, 0.4, 0.3, 0.1\}$. Finally, in the presence of noisy data (which is more realistic in practice) all numerical experiments are revisited with an introduction of Gaussian noise with various values of the standard deviation about the *true* displacement.

4.1. Inversion without noise

4.1.1. The coefficient $\beta_1 = 0$

Figs. 2 to 6 show the history of estimating the prestress S_0^{true} with different initial guesses $S_0 = 0.5G, G$ and $2G$ using the presented algorithm. The final estimates of S_0^{true} and corresponding relative errors in all cases are summarized in Tab. 2. It can be seen that all initial guesses converge to the correct result with acceptable errors. It is also clear that the bigger difference between the target value and the initial guess requires a higher number of iterations toward convergence.

Algorithm 1 Initial stress S_0 inversion scheme

```
Set iteration counter n ← 1
Set S_0 ← initial guess
Set step length ΔS_0
Compute v_m via Eq. (50)
Compute misfit F via Eq. (51)
Set convergence tolerance TOL
Set maximum number of iterations maxiter
while F > TOL and n < maxiter do
    Solve the state problem to obtain k_j and V_j via Eq. (57) and Eq. (58)
    Compute v_p via Eq. (50)
    Solve the adjont problem to obtain λ_j and φ_j via Eq. (63)
    Compute grad S_0 via Eq. (65)
    if v_p − v_m > 0 then
        Update S_0 ← S_0 + ΔS_0 grad S_0
    else
        Update S_0 ← S_0 − ΔS_0 grad S_0
    end if
    Compute misfit F via Eq. (51)
    n ← n + 1
end while
```

Table 1: Parameters for numerical examples

	without noise			with noise		
Tolerance	10^{-11}			10^{-8}		
β_1	0 (Sec 4.1.1)	-0.5 (Sec 4.1.2)	-0.5 (Sec 4.1.3)	0 (Sec 4.2.1)	-0.5 (Sec 4.2.2)	-0.5 (Sec 4.2.3)
ΔS_0	1×10^{-5}	3×10^{-5}	2×10^{-5}	7×10^{-7}	2×10^{-6}	2×10^{-6}

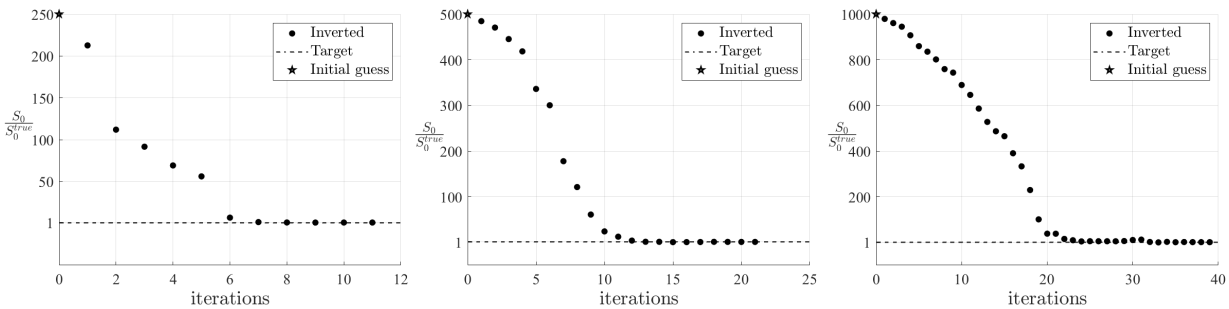

Figure 2: $\beta_1 = 0$ and the target value $S_0^{\text{true}} = 2 \times 10^{-3} G$; the initial guess $S_0 = 0.5G$ (left), $S_0 = G$ (center), and $S_0 = 2G$ (right).

4.1.2. The coefficient $\beta_1 = -0.5$

Now, all parameters are the same as before, except that $\beta_1 = -0.5$. Figs. 7 to 11 and Tab. 3 show a great performance of our proposed inversion in predicting the prestress S_0^{true}.

4.1.3. Different excitation frequencies

Next, when $\beta_1 = -0.5$ a set of four decreasing frequencies $\omega \in \{0.5, 0.4, 0.3, 0.1\}$ and the initial guesses $S_0 = G, 2G$ are used to track the reductions of the misfit and the absolute difference $|S_0 - S_0^{\text{true}}|$ versus the number of iterations. The

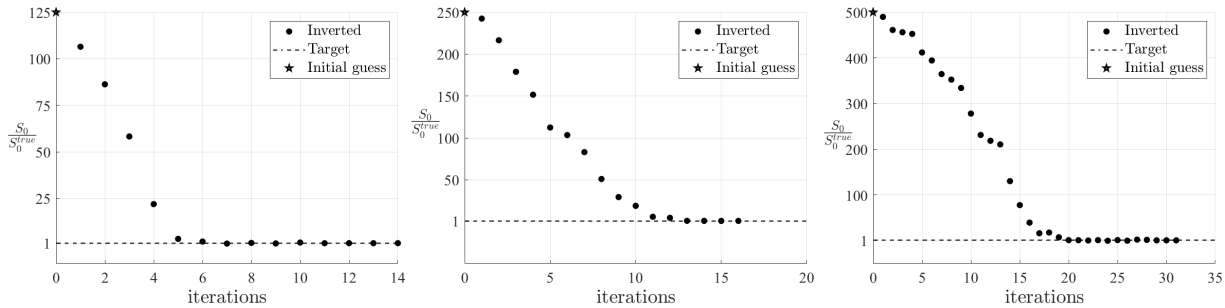

Figure 3: $\beta_1 = 0$ and the target value $S_0^{\text{true}} = 4 \times 10^{-3}G$; the initial guess $S_0 = 0.5G$ (left), $S_0 = G$ (center), and $S_0 = 2G$ (right).

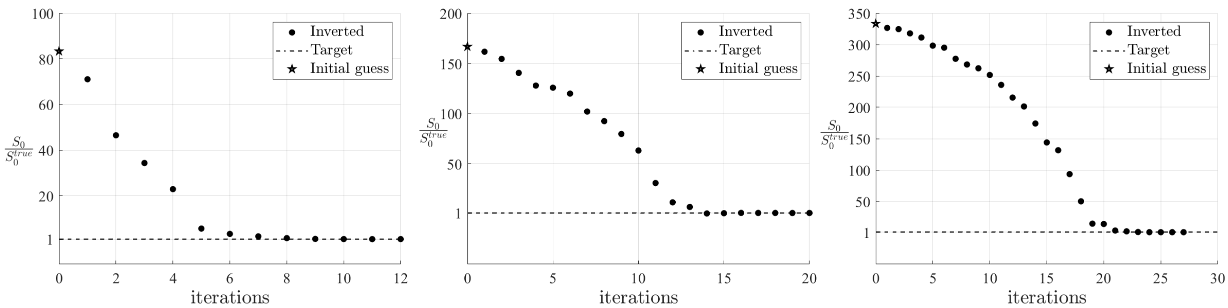

Figure 4: $\beta_1 = 0$ and the target value $S_0^{\text{true}} = 6 \times 10^{-3}G$; the initial guess $S_0 = 0.5G$ (left), $S_0 = G$ (center), and $S_0 = 2G$ (right).

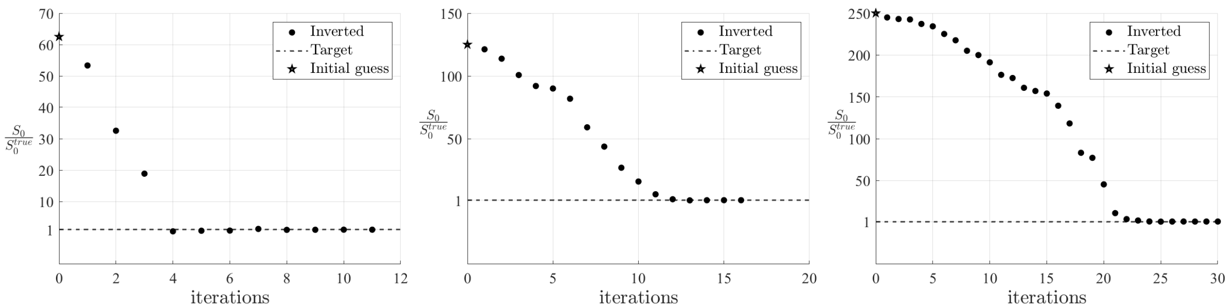

Figure 5: $\beta_1 = 0$ and the target value $S_0^{\text{true}} = 8 \times 10^{-3}G$; the initial guess $S_0 = 0.5G$ (left), $S_0 = G$ (center), and $S_0 = 2G$ (right).

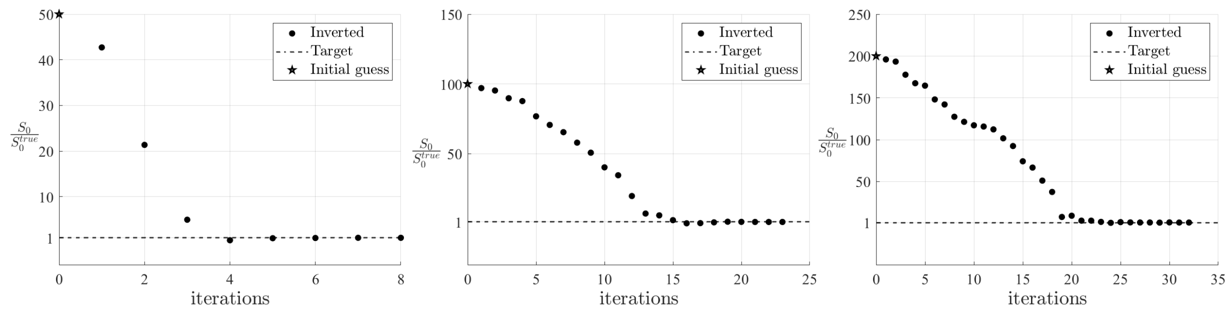

Figure 6: $\beta_1 = 0$ and the target value $S_0^{\text{true}} = 10 \times 10^{-3}G$; the initial guess $S_0 = 0.5G$ (left), $S_0 = G$ (center), and $S_0 = 2G$ (right).

Table 2: $\beta_1 = 0$; Final prediction value of the prestress S_0^{pred} with three initial guesses.

S_0^{true}/G	Initial $S_0 = 0.5G$		Initial $S_0 = G$		Initial $S_0 = 2G$	
	S_0^{pred}/G	Rel. err. (%)	S_0^{pred}/G	Rel. err. (%)	S_0^{pred}/G	Rel. err. (%)
2×10^{-3}	2.0061×10^{-3}	0.3064	2.0008×10^{-3}	0.0384	1.9681×10^{-3}	1.5958
4×10^{-3}	3.9752×10^{-3}	0.6189	3.9821×10^{-3}	0.4476	3.8588×10^{-3}	3.5288
6×10^{-3}	6.0119×10^{-3}	0.0197	5.9978×10^{-3}	0.0363	5.9479×10^{-3}	0.8679
8×10^{-3}	7.9973×10^{-3}	0.0331	7.9765×10^{-3}	0.0293	8.0483×10^{-3}	0.6032
10×10^{-3}	10.001×10^{-3}	0.0102	9.9697×10^{-3}	0.3029	9.9876×10^{-3}	0.1242

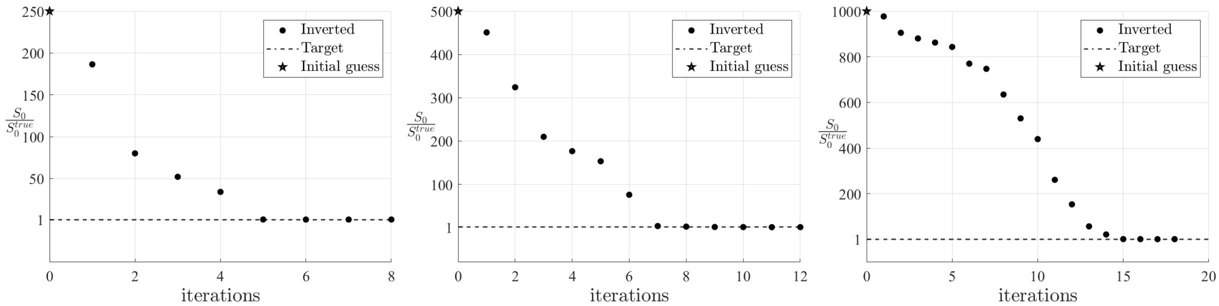

Figure 7: $\beta_1 = -0.5$ and the target value $S_0^{\text{true}} = 2 \times 10^{-3}G$; the initial guess $S_0 = 0.5G$ (left), $S_0 = G$ (center), and $S_0 = 2G$ (right).

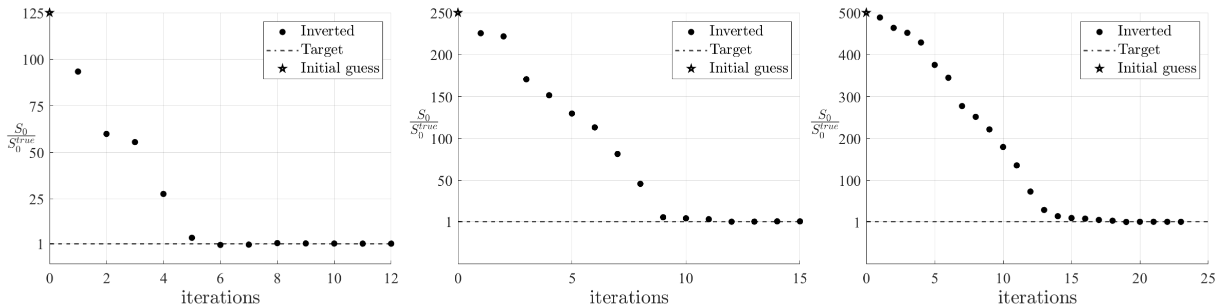

Figure 8: $\beta_1 = -0.5$ and the target value $S_0^{\text{true}} = 4 \times 10^{-3}G$; the initial guess $S_0 = 0.5G$ (left), $S_0 = G$ (center), and $S_0 = 2G$ (right).

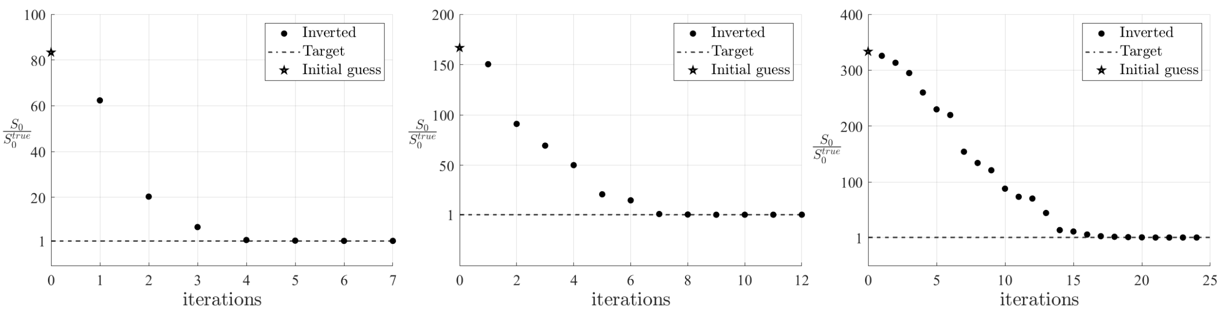

Figure 9: $\beta_1 = -0.5$ and the target value $S_0^{\text{true}} = 6 \times 10^{-3}G$; the initial guess $S_0 = 0.5G$ (left), $S_0 = G$ (center), and $S_0 = 2G$ (right).

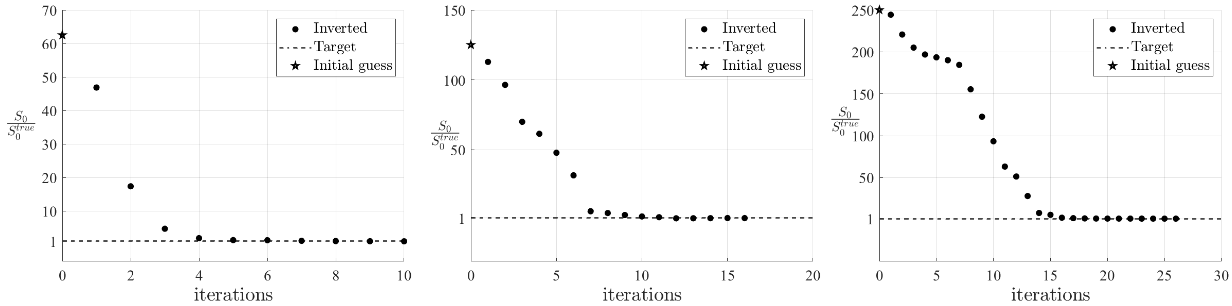

Figure 10: $\beta_1 = -0.5$ and the target value $S_0^{\text{true}} = 8 \times 10^{-3}G$; the initial guess $S_0 = 0.5G$ (left), $S_0 = G$ (center), and $S_0 = 2G$ (right).

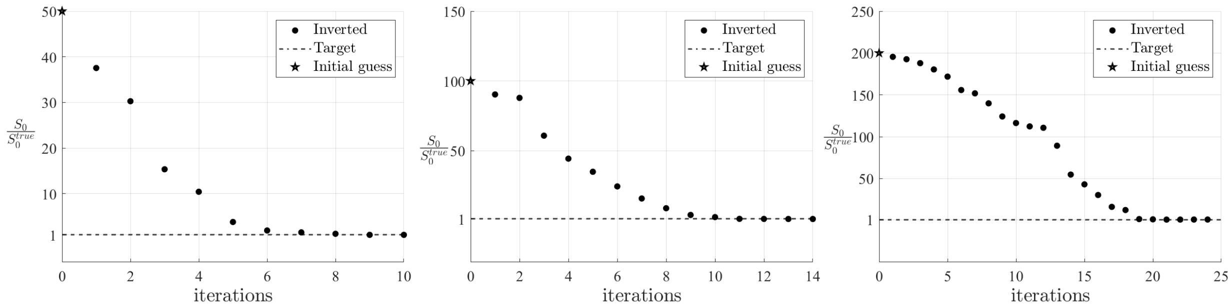

Figure 11: $\beta_1 = -0.5$ and the target value $S_0^{\text{true}} = 10 \times 10^{-3}G$; the initial guess $S_0 = 0.5G$ (left), $S_0 = G$ (center), and $S_0 = 2G$ (right).

Table 3: $\beta_1 = -0.5$; Final prediction value of the prestress S_0^{pred} with three initial guesses.

S_0^{true}/G	Initial $S_0 = 0.5G$		Initial $S_0 = G$		Initial $S_0 = 2G$	
	S_0^{pred}/G	Rel. err. (%)	S_0^{pred}/G	Rel. err. (%)	S_0^{pred}/G	Rel. err. (%)
2×10^{-3}	1.9780×10^{-3}	1.0995	1.9993×10^{-3}	0.0351	1.9463×10^{-3}	2.6852
4×10^{-3}	4.0092×10^{-3}	0.2308	4.0789×10^{-3}	1.9730	3.9832×10^{-3}	0.4209
6×10^{-3}	5.9955×10^{-3}	0.0074	5.9147×10^{-3}	1.4224	6.0170×10^{-3}	0.2837
8×10^{-3}	7.9577×10^{-3}	0.5293	7.9210×10^{-3}	0.9876	7.9826×10^{-3}	0.2173
10×10^{-3}	9.9349×10^{-3}	0.6508	9.9985×10^{-3}	0.0149	9.9697×10^{-3}	0.3028

decrease of the misfit value for each frequency is separated by vertical and dashed lines. Fig. 12 shows the reductions of the misfit, and the difference of target and detected values through the inversion scheme for each frequency.

4.2. Inversion with noise

In a real situation, measurement equipment always is affected by a variety of sources which creates noise. Then the observed data contains both the physical response and the noise, given by:

$$v_{ob} = v_m \times noise. \tag{68}$$

where $noise = normrnd(\mu, \sigma)$. In Matlab, the *normrnd* function generates a random number from the normal distribution with mean parameter μ and standard deviation σ.

In order to demonstrate the algorithmic performance of the presented procedure, besides being interesting in noise-free experiments, we next consider numerical examples in section 4.1 with only one target value $S_0^{true} = 5 \times 10^{-3}G$, but the measurement data is noisy. In our cases, we choose $\mu = 1$ and three ascending numbers of standard deviation $\sigma = \{0.5\%, 1\%, 1.5\%\}$ for generating the noise.

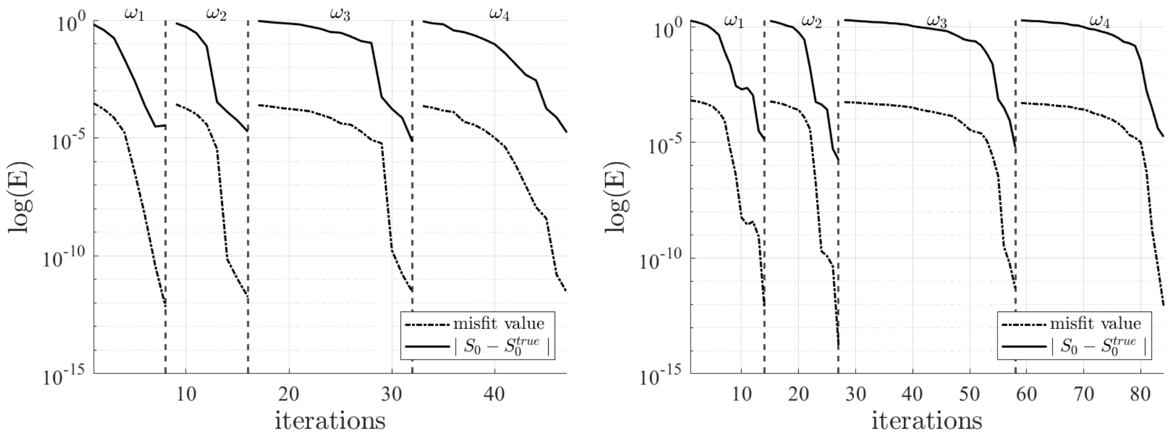

Figure 12: $\beta_1 = -0.5$ and the target value $S_0^{\text{true}} = 5 \times 10^{-3}G$; the initial guess $S_0 = G$ (left) and $S = 2G$ (right) with four excited frequencies $\omega_1 = 0.5, \omega_2 = 0.4, \omega_3 = 0.3, \omega_4 = 0.1$.

4.2.1. *The coefficient* $\beta_1 = 0$

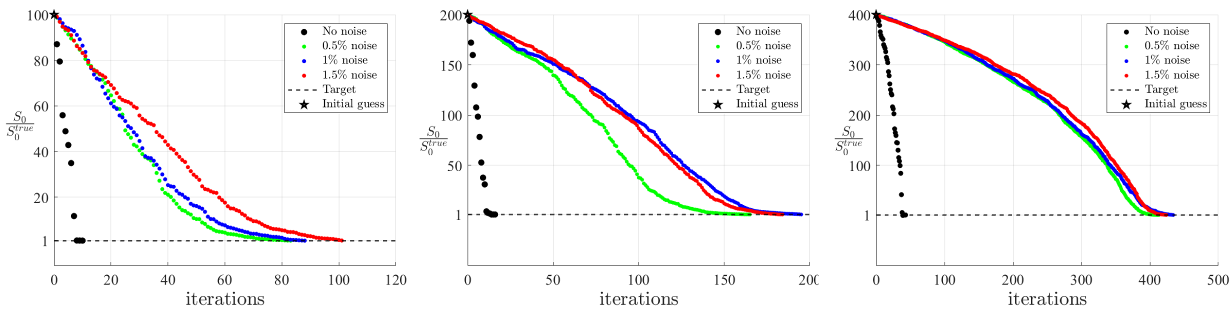

Figure 13: $\beta_1 = 0$ and the target value $S_0^{\text{true}} = 5 \times 10^{-3}G$, the initial guess $S_0 = 0.5G$ (left), $S_0 = G$ (center), and $S_0 = 2G$ (right).

As shown in the Fig. 13 and Table 4, for measurement data associated with the three levels of noise, the algorithm successfully recovers the prestress profile in both case initial guess $S_0 = G$ and $S_0 = 2G$. Moreover, for higher level of noise, the algorithm needs a larger number of iterations to reach target value.

Table 4: $\beta_1 = 0$; Final prediction value of the prestress S_0^{pred} with noise, three initial guesses, $S_0^{\text{true}}/G = 5 \times 10^{-3}$.

Noise	Initial $S_0 = 0.5G$		Initial $S_0 = G$		Initial $S_0 = 2G$	
	S_0^{pred}/G	Rel. err. (%)	S_0^{pred}/G	Rel. err. (%)	S_0^{pred}/G	Rel. err. (%)
0.5%	4.9274×10^{-3}	1.4523	5.0589×10^{-3}	1.1788	4.9772×10^{-3}	0.4565
1%	4.8902×10^{-3}	2.1970	5.0801×10^{-3}	1.6011	5.1211×10^{-3}	2.4211
1.5%	5.2167×10^{-3}	4.3347	4.8835×10^{-3}	2.3292	4.8426×10^{-3}	3.1471

4.2.2. *The coefficient* $\beta_1 = -0.5$

This example shares the familiar setting parameters as before, except that $\beta_1 = -0.5$. The convergence of the proposed inversion and corresponding relative errors in all cases can be observed in Fig. 14 and Table 5 respectively. As can be seen, for the low level of noise, the algorithm successfully converges to the target value after several iterations. Additionally, the number of iterations is proportional to the level of noise, and all values of the ratio of S_0/S_0^{true} converges to the desired value of 1.

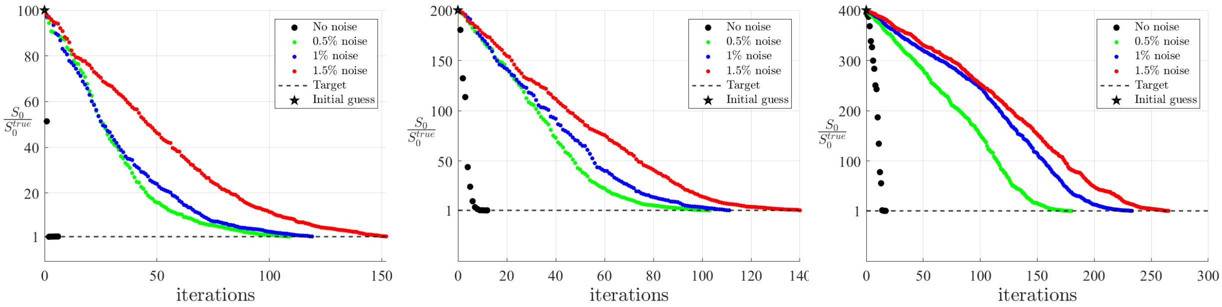

Figure 14: $\beta_1 = -0.5$ and the target value $S_0^{\text{true}} = 5 \times 10^{-3}G$, the initial guess $S = 0.5G$ (left), $S = G$ (center), and $S = 2G$ (right).

Table 5: $\beta_1 = -0.5$; Final prediction value of the prestress S_0^{pred} with noise, three initial guesses, $S_0^{\text{true}}/G = 5 \times 10^{-3}$.

Noise	Initial $S_0 = 0.5G$		Initial $S_0 = G$		Initial $S_0 = 2G$	
	S_0^{pred}/G	Rel. err. (%)	S_0^{pred}/G	Rel. err. (%)	S_0^{pred}/G	Rel. err. (%)
0.5%	5.0956×10^{-3}	1.9128	4.9249×10^{-3}	1.5015	5.1204×10^{-3}	2.4082
1%	5.1501×10^{-3}	3.0029	5.1658×10^{-3}	3.3156	4.8473×10^{-3}	3.0536
1.5%	5.1704×10^{-3}	3.4070	5.2175×10^{-3}	4.3508	5.2242×10^{-3}	4.4837

4.2.3. Different excited frequencies

Next, to examine the effectiveness of the proposed algorithm, all parameters are as in 4.1.3, but the measured displacement contains noise by assuming standard deviation $\sigma = 1\%$ in Eq. (68). Overall, due to the noise, the reduction of misfit and $|S_0 - S_0^{true}|$ value at each frequency takes greater number of iterations than in noise-free cases. Fig. 15 shows that, in the presence of noise, the algorithm returns acceptable results of misfit value and $|S_0 - S_0^{true}|$ for all frequencies.

5. Conclusion

In this paper, we have described a rather simple approach to detect the level of prestress in elastic circular cross-section rods of finite length based on their torsional response using dispersion-constrained inversion. In this methodology, we invoke the forward quadratic eigenvalue problem as a physical constraint of the misfit function. In the forward problem, the hyper element, including our simplifications, helps us reduce spatial discretization of the rod from three dimensions to only one, leading to computational savings. Regarding the quadratic eigenvalue problem, we provide the closed-form expression of component matrices, resulting in a straighforward implementation of the proposed hyper element. The saving of computational cost is especially meaningful in the inverse problem due to the requirement of solving the forward problem in every single iteration. The inversion procedure is examined with various true values of prestress, frequency and multiple initial guesses in each case. The reported numerical results illustrate the capacity of the proposed approach in detecting the initial stress with satisfactory accuracy. Moreover, the algorithm can be used to predict fairly accurately the target value even in the presence of noise in the measured displacement data.

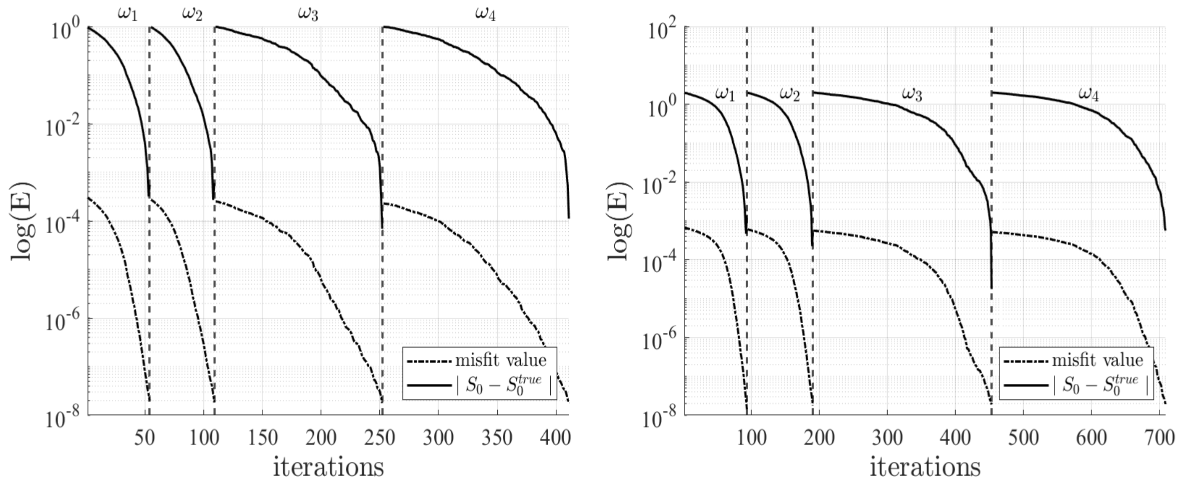

Figure 15: $\beta_1 = -0.5$ and the target value $S_0^{\text{true}} = 5 \times 10^{-3}G$, the initial guess $S_0 = G$ (left), and $S_0 = 2G$ (right), $\sigma = 1\%$, with four excited frequencies $\omega_1 = 0.5$, $\omega_2 = 0.4$, $\omega_3 = 0.3$, $\omega_4 = 0.1$.

Appendix A. Lemma

We will show how to take the derivative of the following *real-valued function* with respect to s:

$$f(z) = \frac{1}{2}|z|^2, \tag{A.1}$$

where $z = z(s) = u(s) + \mathrm{i}v(s)$, $u(s)$ and $v(s)$ are real-valued functions of the real independent variable s.

First, utilizing the conjugate complex variable, we are able to rewrite the function f as follows:

$$2f(z) = |z|^2 = z\bar{z}. \tag{A.2}$$

Taking the derivatives of both sides with respect to s, we obtain

$$2f'(z) = \frac{df}{ds} = z'\bar{z} + z\bar{z}' = (u' + \mathrm{i}v')(u - \mathrm{i}v) + (u + \mathrm{i}v)(u' - \mathrm{i}v') = 2(uu' + vv') = 2\mathrm{Re}(z\bar{z}'). \tag{A.3}$$

It follows immediately that

$$f'(z) = \mathrm{Re}(z\bar{z}'). \tag{A.4}$$

Appendix B. Gradient of the objective function

Let us recall the Lagrangian function used in solving the inverse problem:

$$L := F + C = \frac{1}{2}\left|v_m(0, R;\ \omega) - v_p(0, R;\ \omega)\right|^2 + C, \tag{B.1}$$

The main goal here is to obtain the derivative of the misfit part F with respect to the prestress S_0. Specifically, F can be considered as a function of the complex variable $z = v_m(0, R;\ \omega) - v_p(0, R;\ \omega)$, i.e., $F(z) = |z|^2/2$. Therefore, its gradient with respect to S_0 can be determined by using Eq. (A.4) as follows:

$$\frac{\partial F}{\partial S_0} = \mathrm{Re}\left[\frac{\partial\left(\overline{v_m - v_p}\right)}{\partial S_0}\left(v_m - v_p\right)\right] = \mathrm{Re}\left[\left(\frac{\partial \overline{v_p}}{\partial S_0}\right)\left(v_p - v_m\right)\right] = \mathrm{Re}\left[\left(\frac{\partial v_p}{\partial S_0}\right)\left(\overline{v_p - v_m}\right)\right], \tag{B.2}$$

where the overline symbol $\bar{(\cdot)}$ denotes the conjugate of a complex number.

Substituting Eq. (44) into Eq. (50), the outermost circumferential displacement at $z = 0$, $\mathcal{V}_{1,N+1}$, can be expressed in terms of the wavenumbers and modeshapes as:

$$v_p\left(r = R_{N+1}, z = 0\right) = \frac{1}{2\pi}\sum_{i=1}^{N+1}\left[\sum_{j=1}^{N+1} V_j \frac{tan\left(k_j L\right)}{k_j} V'_{ji}\right] a'_{i,N+1}. \tag{B.3}$$

Using Eq. (B.3), the derivative of v_p with respect to the prestress S_0 can be determined as:

$$\begin{aligned}\frac{\partial v_p}{\partial S_0} &= \frac{1}{2\pi}\sum_{i=1}^{N+1}\left(\sum_{j=1}^{N+1}\frac{\partial V_j}{\partial S_0}\frac{tan\left(k_j L\right)}{k_j}V'_{ji}\right)a'_{i,N+1} \\ &+ \frac{1}{2\pi}\sum_{i=1}^{N+1}\left(\sum_{j=1}^{N+1} V_j \frac{k_j L sec^2\left(k_j L\right) - tan\left(k_j L\right)}{k_j^2}\frac{\partial k_j}{\partial S_0}V'_{ji}\right)a'_{i,N+1} \\ &= \frac{1}{2\pi}\sum_{i=1}^{N+1}\left(\sum_{j=1}^{N+1}\frac{\partial V_j}{\partial S_0}H_{1j}V'_{ji}\right)a'_{i,N+1} + \frac{1}{2\pi}\sum_{i=1}^{N+1}\left(\sum_{j=1}^{N+1}V_j H_{2j}\frac{\partial k_j}{\partial S_0}V'_{ji}\right)a'_{i,N+1},\end{aligned} \tag{B.4}$$

where

$$H_{1j} = \frac{tan\left(k_j L\right)}{k_j}, \qquad H_{2j} = \frac{k_j L sec^2\left(k_j L\right) - tan\left(k_j L\right)}{k_j^2}, \tag{B.5}$$

and

$$\begin{bmatrix} \dfrac{\partial V_j}{\partial S_0} \\[2ex] \dfrac{\partial k_j}{\partial S_0} \end{bmatrix} = \begin{bmatrix} \boldsymbol{W}^T & 0 \\ 0 & 1 \end{bmatrix} \begin{bmatrix} \dfrac{\partial \boldsymbol{V}_j}{\partial S_0} \\[2ex] \dfrac{\partial k_j}{\partial S_0} \end{bmatrix}, \tag{B.6}$$

where $\boldsymbol{W}$ has unit value only for the displacement at $r = R$, whereas the other elements are null.

The derivatives $\dfrac{\partial \boldsymbol{V}_j}{\partial S_0}$ and $\dfrac{\partial k_j}{\partial S_0}$ of the j^{th} eigenvectors and eigenvalues can be obtained from the two constraints incorporated in the Lagrangian function

1. *Quadratic eigenvalue problem:* The equation for the j^{th} eigenmode can be expressed as

$$\left(k_j^2\boldsymbol{A} + \boldsymbol{G} - \omega^2\boldsymbol{M}\right)\boldsymbol{V}_j = \boldsymbol{0}, \quad j = \overline{1, N+1}. \tag{B.7}$$

2. *Normalization condition:* The eigenvector $\boldsymbol{V}_j$ for the j^{th} eigenmode is normalized to satisfy:

$$\boldsymbol{V}_j^T\boldsymbol{A}\boldsymbol{V}_j = 1, \quad j = \overline{1, N+1}. \tag{B.8}$$

Differentiating both sides of Eqs. (B.7) & (B.8) with respect to S_0 leads to

$$\left(k_j^2\boldsymbol{A} + \boldsymbol{G} - \omega^2\boldsymbol{M}\right)\frac{\partial \boldsymbol{V}_j}{\partial S_0} + 2k_j\boldsymbol{A}\boldsymbol{V}_j\frac{\partial k_j}{\partial S_0} = -\left[k_j^2\frac{\partial \boldsymbol{A}}{\partial S_0} + \frac{\partial\left(\boldsymbol{G} - \omega^2\boldsymbol{M}\right)}{\partial S_0}\right]\boldsymbol{V}_j = -k_j^2\frac{\partial \boldsymbol{A}}{\partial S_0}\boldsymbol{V}_j. \tag{B.9}$$

$$2k_j\boldsymbol{V}_j^T\boldsymbol{A}\frac{\partial \boldsymbol{V}_j}{\partial S_0} + \left(\boldsymbol{V}_j^T\boldsymbol{A}\boldsymbol{V}_j - 1\right)\frac{\partial k_j}{\partial S_0} = \frac{-1}{2}\boldsymbol{V}_j^T\left(2k_j\frac{\partial \boldsymbol{A}}{\partial S_0}\right)\boldsymbol{V}_j = -k_j\boldsymbol{V}_j^T\frac{\partial \boldsymbol{A}}{\partial S_0}\boldsymbol{V}_j. \tag{B.10}$$

Rearranging these two equations, the derivatives $\dfrac{\partial \boldsymbol{V}_j}{\partial S_0}$ and $\dfrac{\partial k_j}{\partial S_0}$ can be obtained by solving the following system of equations:

$$\begin{bmatrix} k_j^2\boldsymbol{A}+\boldsymbol{G}-\omega^2\boldsymbol{M} & 2k_j\boldsymbol{A}\boldsymbol{V}_j \\ 2k_j\boldsymbol{V}_j^T\boldsymbol{A} & \boldsymbol{V}_j^T\boldsymbol{A}\boldsymbol{V}_j-1 \end{bmatrix}\begin{bmatrix} \dfrac{\partial \boldsymbol{V}_j}{\partial S_0} \\ \\ \dfrac{\partial k_j}{\partial S_0} \end{bmatrix} = -\begin{bmatrix} k_j^2\dfrac{\partial \boldsymbol{A}}{\partial S_0}\boldsymbol{V}_j \\ \\ k_j\boldsymbol{V}_j^T\dfrac{\partial \boldsymbol{A}}{\partial S_0}\boldsymbol{V}_j \end{bmatrix} \tag{B.11}$$

Thus,

$$\begin{bmatrix} \dfrac{\partial \boldsymbol{V}_j}{\partial S_0} \\ \\ \dfrac{\partial k_j}{\partial S_0} \end{bmatrix} = -\begin{bmatrix} k_j^2\boldsymbol{A}+\boldsymbol{G}-\omega^2\boldsymbol{M} & 2k_j\boldsymbol{A}\boldsymbol{V}_j \\ 2k_j\boldsymbol{V}_j^T\boldsymbol{A} & \boldsymbol{V}_j^T\boldsymbol{A}\boldsymbol{V}_j-1 \end{bmatrix}^{-1}\begin{bmatrix} k_j^2\dfrac{\partial \boldsymbol{A}}{\partial S_0}\boldsymbol{V}_j \\ \\ k_j\boldsymbol{V}_j^T\dfrac{\partial \boldsymbol{A}}{\partial S_0}\boldsymbol{V}_j \end{bmatrix} \tag{B.12}$$

Then, substituting Eq.(B.12) into Eq.(B.6) results in

$$\begin{bmatrix} \dfrac{\partial V_j}{\partial S_0} \\ \\ \dfrac{\partial k_j}{\partial S_0} \end{bmatrix} = -\begin{bmatrix} \boldsymbol{W}^T & 0 \\ 0 & 1 \end{bmatrix}\begin{bmatrix} k_j^2\boldsymbol{A}+\boldsymbol{G}-\omega^2\boldsymbol{M} & 2k_j\boldsymbol{A}\boldsymbol{V}_j \\ 2k_j\boldsymbol{V}_j^T\boldsymbol{A} & \boldsymbol{V}_j^T\boldsymbol{A}\boldsymbol{V}_j-1 \end{bmatrix}^{-1}\begin{bmatrix} k_j^2\dfrac{\partial \boldsymbol{A}}{\partial S_0}\boldsymbol{V}_j \\ \\ k_j\boldsymbol{V}_j^T\dfrac{\partial \boldsymbol{A}}{\partial S_0}\boldsymbol{V}_j \end{bmatrix}, \tag{B.13}$$

Next, plugging Eq.(B.13) into Eq.(B.4) gives us

$$\begin{aligned}
&\left(\frac{\partial v_p}{\partial S_0}\right)\left(\overline{v_p - v_m}\right) \\
&= \frac{-1}{2\pi}\left\{\begin{bmatrix} k_j^2\boldsymbol{A}+\boldsymbol{G}-\omega^2\boldsymbol{M} & 2k_j\boldsymbol{A}\boldsymbol{V}_j \\ 2k_j\boldsymbol{V}_j^T\boldsymbol{A} & \boldsymbol{V}_j^T\boldsymbol{A}\boldsymbol{V}_j-1 \end{bmatrix}^{-1}\begin{bmatrix} \sum_{i=1}^{N+1}\left(\sum_{j=1}^{N+1} H_{1j}V'_{ji}\right)a'_{i,N+1}\left(\overline{v_p - v_m}\right)\boldsymbol{W} \\ \sum_{i=1}^{N+1}\left(\sum_{j=1}^{N+1} V_jH_{2j}V'_{ji}\right)a'_{i,N+1}\left(\overline{v_p - v_m}\right) \end{bmatrix}\right\}^T \\
&\times\begin{bmatrix} k_j^2\dfrac{\partial \boldsymbol{A}}{\partial S_0}\boldsymbol{V}_j \\ \\ k_j\boldsymbol{V}_j^T\dfrac{\partial \boldsymbol{A}}{\partial S_0}\boldsymbol{V}_j \end{bmatrix} &\text{(B.14)} \\
&= \sum_{j=1}^{N+1}\begin{bmatrix} \boldsymbol{\lambda}_j^T & \varphi_j \end{bmatrix}\begin{bmatrix} k_j^2\dfrac{\partial \boldsymbol{A}}{\partial S_0}\boldsymbol{V}_j \\ \\ k_j\boldsymbol{V}_j^T\dfrac{\partial \boldsymbol{A}}{\partial S_0}\boldsymbol{V}_j \end{bmatrix}, &\text{(B.15)}
\end{aligned}$$

where $\boldsymbol{\lambda}_j$ is a vector of Lagrange multipliers, and φ_j is a scalar Lagrange multiplier.

$$\begin{bmatrix} \boldsymbol{\lambda}_j \\ \varphi_j \end{bmatrix} = \frac{-1}{2\pi}\begin{bmatrix} k_j^2\boldsymbol{A}+\boldsymbol{G}-\omega^2\boldsymbol{M} & 2k_j\boldsymbol{A}\boldsymbol{V}_j \\ 2k_j\boldsymbol{V}_j^T\boldsymbol{A} & \boldsymbol{V}_j^T\boldsymbol{A}\boldsymbol{V}_j-1 \end{bmatrix}^{-1}\begin{bmatrix} \sum_{i=1}^{N+1}\left(\sum_{j=1}^{N+1} H_{1j}V'_{ji}\right)a'_{i,N+1}\left(\overline{v_p - v_m}\right)\boldsymbol{W} \\ \sum_{i=1}^{N+1}\left(\sum_{j=1}^{N+1} V_jH_{2j}V'_{ji}\right)a'_{i,N+1}\left(\overline{v_p - v_m}\right) \end{bmatrix} \tag{B.16}$$

Finally, the gradient in Eq.(B.2 can be expressed in terms of Lagrange multipliers as:

$$\frac{\partial F}{\partial S_0} = \mathrm{Re}\left\{\sum_{j=1}^{N+1} k_j^2\boldsymbol{\lambda}_j^T\frac{\partial \boldsymbol{A}}{\partial S_0}\boldsymbol{V}_j + k_j\varphi_j\boldsymbol{V}_j^T\frac{\partial \boldsymbol{A}}{\partial S_0}\boldsymbol{V}_j\right\}, \quad j = \overline{1, N+1}. \tag{B.17}$$

References

[1] M. Biot, Increase of torsional stiffness of a prismatic bar due to axial tension, J. Appl. Phys. 10 (1939) 860–864.
[2] M. Biot, The influence of initial stress on elastic waves, J. Appl. Phys. 11 (1940) 522–530.
[3] M. Biot, Mechanics of Incremental Deformations, JohnWiley and Sons, Inc., 1965.
[4] M. Destrade, R. Ogden, On stress-dependent elastic moduli and wave speeds, J. Appl.Math. 78 (2013) 965–997.
[5] M. Shams, M. Destrade, R. Ogden, Initial stresses in elastic solids: constitutive laws and acoustoelasticity,Wave Motion 48 (2011) 552–567.
[6] M. Tadi, Explicit method for inverse wave scattering in solids, Inverse Problems 13 (1997) 509-521.
[7] Na, SW., Kallivokas, L.F. On the inverse problem of soil profile reconstruction: a comparison of time-domain approaches, Computational Mechanics 42, 921 (2008).
[8] Karve, P.M., Na, SW., Kang, J.W. et al. The inverse medium problem for Timoshenko beams and frames: damage detection and profile reconstruction in the time-domain, Computational Mechanics 47, 117–136 (2011).
[9] Arash Fathi, Loukas F. Kallivokas, Babak Poursartip, Full-waveform inversion in three-dimensional PML-truncated elastic media, Computer Methods in Applied Mechanics and Engineering, v296, 2015, pp. 39-72.
[10] Mashayekh H, Kallivokas LF, Tassoulas JL. Parameter estimation in layered media using dispersion-constrained inversion. J Eng Mech 2018;144(11):04018099.
[11] Jin Ho Lee, Se-Hyeok Lee, Full waveform inversion to estimate the material properties of a layered half-space, Soil Dynamics and Earthquake Engineering, v151, 2021, 106956. https://doi.org/10.1016/j.soildyn.2021.106956.
[12] Sedef Kocakaplan, John L. Tassoulas, Wave propagation in initially-stressed elastic rods, Journal of Sound and Vibration, v443, 2019, pp. 293-309. https://doi.org/10.1016/j.jsv.2018.11.045.
[13] Sedef Kocakaplan, John L. Tassoulas, Torsional response of pretensioned elastic rods, International Journal of Solids and Structures, v191–192, 2020, pp. 1-7. https://doi.org/10.1016/j.ijsolstr.2020.02.004
[14] Waas, G. 1972. "Linear two-dimensional analysis of soil dynamics problems in semi-infinite layered media." Ph.D. dissertation, Dept. of Civil Engineering, Univ. of California, Berkeley.
[15] Kausel, E. 1981. An explicit solution for the green functions for dynamic loads in layered media. Cambridge, MA: Massachusetts Institute of Technology.